

# Ultralong afterglow and unity quantum yield from a transparent CsCdCl<sub>3</sub>: Mn crystal

Yeqi Liu<sup>1</sup>, Xiangzhou Zhang<sup>1</sup>, Xiaojia Wang<sup>1</sup>, Shao Yan<sup>1</sup>, Yanjie Liang<sup>1</sup>, and Yuhai Zhang<sup>1</sup>

<sup>1</sup>Affiliation not available

January 9, 2023

## Abstract

Transparent afterglow crystals are keenly desired for three-dimensional information storage. Herein, CsCdCl<sub>3</sub> perovskite crystals were grown by a programmable cooling procedure in a hydrothermal reactor. The pristine crystal showed an abnormal optical behavior where the absorption increased by 2.3 folds at high temperature, leading to a 4-fold boost of PL intensity. After Mn<sup>2+</sup> doping, the PL QY was improved to nearly unity. Importantly, the doped crystals exhibited an ultralong afterglow up to 12 hours after ceasing UV excitation and a high transmittance up to 75% in the visible region. This work brought a new member to the library of transparent afterglow crystal, opening up many possibilities to advanced applications such as volumetric display and three-dimensional information encryption.

## Ultralong Afterglow and Unity Quantum Yield from a Transparent CsCdCl<sub>3</sub>: Mn Crystal

*Yeqi Liu<sup>1</sup>; Xiangzhou Zhang<sup>1</sup>; Xiaojia Wang<sup>1</sup>; Shao Yan<sup>2</sup>; Yanjie Liang<sup>2</sup>; Yuhai Zhang<sup>1,\*</sup>*

<sup>1</sup>Institute for Advanced Interdisciplinary Research (iAIR), School of Chemistry and Chemical Engineering, University of Jinan, Jinan 250022, Shandong, China.

<sup>2</sup>Key Laboratory for Liquid-Solid Structure Evolution and Processing of Materials, Ministry of Education, Shandong University, Jinan 250061, P. R. China.

## AUTHOR INFORMATION

Corresponding Author

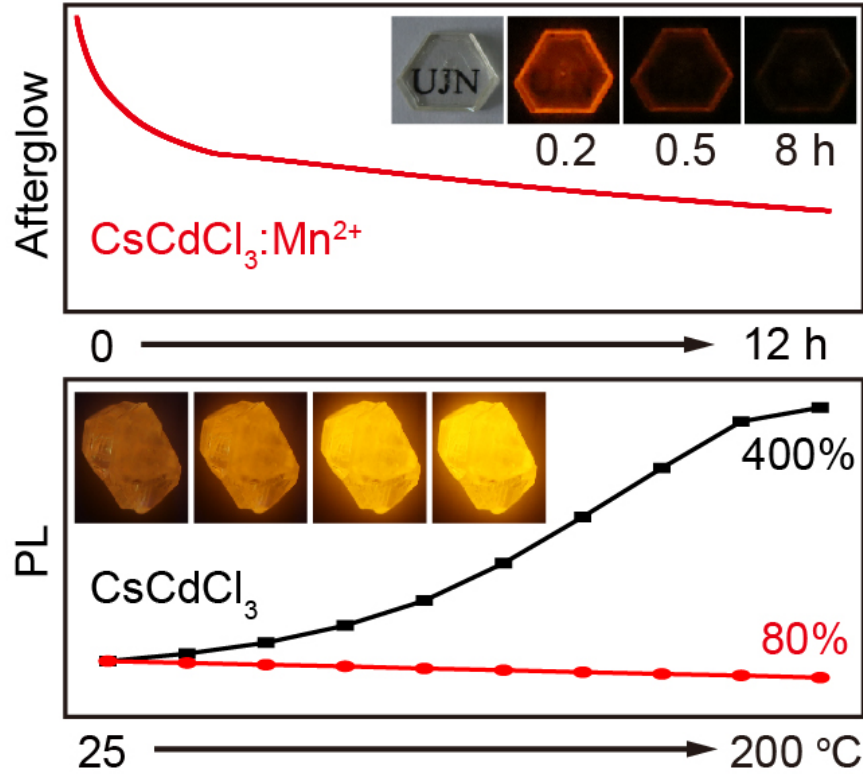
ifc\_zhangyh@ujn.edu.cn

## Abstract

Transparent afterglow crystals are keenly desired for three-dimensional information storage. Herein, CsCdCl<sub>3</sub> perovskite crystals were grown by a programmable cooling procedure in a hydrothermal reactor. The pristine crystal showed an abnormal optical behavior where the absorption increased by 2.3 folds at high temperature, leading to a 4-fold boost of PL intensity. After Mn<sup>2+</sup> doping, the PL QY was improved to nearly unity. Importantly, the doped crystals exhibited an ultralong afterglow up to 12 hours after ceasing UV excitation and a high transmittance up to 75% in the visible region. This work brought a new member to the library of transparent afterglow crystal, opening up many possibilities to advanced applications such as volumetric display and three-dimensional information encryption.

**KEYWORDS:** CsCdCl<sub>3</sub> crystal [?] ultra-long afterglow [?] thermally enhanced luminescence [?] resonant energy transfer [?] transparent afterglow matrix

**TOC:**



## 1. INTRODUCTION

Afterglow phosphors are capable of a long-term storage for varied excitation photons, including X-ray, ultraviolet, and visible light.<sup>[1-6]</sup> Their potential application in information encryption has been widely demonstrated in a two-dimensional (2D) manner such as emergence sign,<sup>[7]</sup> anti-counterfeiting pattern,<sup>[8]</sup> and X-ray imaging screen.<sup>[9]</sup> Up to date, many afterglow materials have been developed such as  $\text{SrAl}_2\text{O}_4:\text{Eu}^{2+}, \text{Dy}^{3+}$ ,<sup>[10]</sup>  $\text{CaS}:\text{Eu}^{2+}, \text{Sm}^{3+}$ ,<sup>[11]</sup>  $\text{SrSi}_2\text{AlO}_2\text{N}_3:\text{Eu}^{2+}, \text{Ln}^{3+}$ .<sup>[12]</sup> These traditional phosphors usually have a high lattice energy, which requires a high temperature calcination procedure to form the target phase. Unfortunately, the calcination process not only increases the production cost but also brings a severe safety risk to the manufacturer. Moreover, it causes unwanted agglomeration of powders that leads to a severe scattering issue.<sup>[13, 14]</sup> This poses a great challenge to the transparency of product and the ensuing application of afterglow phosphors in 3D information storage or volumetric display.

To circumvent the scattering issue, transparent afterglow materials have emerged in the last decade. For instance, Claire et al. synthesized a polycrystalline  $\text{ZnGa}_2\text{O}_4$  ceramic by combining high-energy ball milling, solid-state reaction and spark plasma sintering methods. The maximum of transmittance reached 78% in the near infrared region.<sup>[15]</sup> Tang et al. successfully embedded fluoride nanocrystals into an amorphous glass matrix, which exhibited a high transmittance up to 80%.<sup>[16]</sup> One major caveat of these nanocrystal-based strategies was the low photoluminescence quantum yield and ensuing poor afterglow intensity as a consequence of the abundant quenching sites on the surface. Recently, our group has developed several transparent afterglow crystals based on chloride double perovskite.<sup>[5, 17-20]</sup> Through proper doping of activator ions, the single crystals exhibited a tunable afterglow emission ranging from red to near-infrared light. Thanks to their low phonon energy, the chlorides showed a high quantum efficiency up to 82% and an afterglow duration of 2 hours. In addition, the doping of Tb ions in  $\text{Cs}_2\text{NaScCl}_6$  not only boosted the PL QY up to 98.2%, but also activated an intense green afterglow up to 12 hours after ceasing X-ray excitation.<sup>[20]</sup> Despite these progress, ultraviolet chargeable transparent crystals of long-term afterglow remained elusive.

In this work, a transparent  $\text{CsCdCl}_3$  crystal was grown by programmable cooling method in a hydrothermal reactor. The PL intensity of pristine crystals was significantly by 4 folds by elevating the temperature from 25 °C to 200 °C. Such abnormal behavior was investigated and ascribed mainly to the thermal enhanced absorption. After  $\text{Mn}^{2+}$  doping, the PL QY exhibited a dramatical increase to nearly unity. Importantly, an ultra-long afterglow over 12-hour was activated under UV excitation.

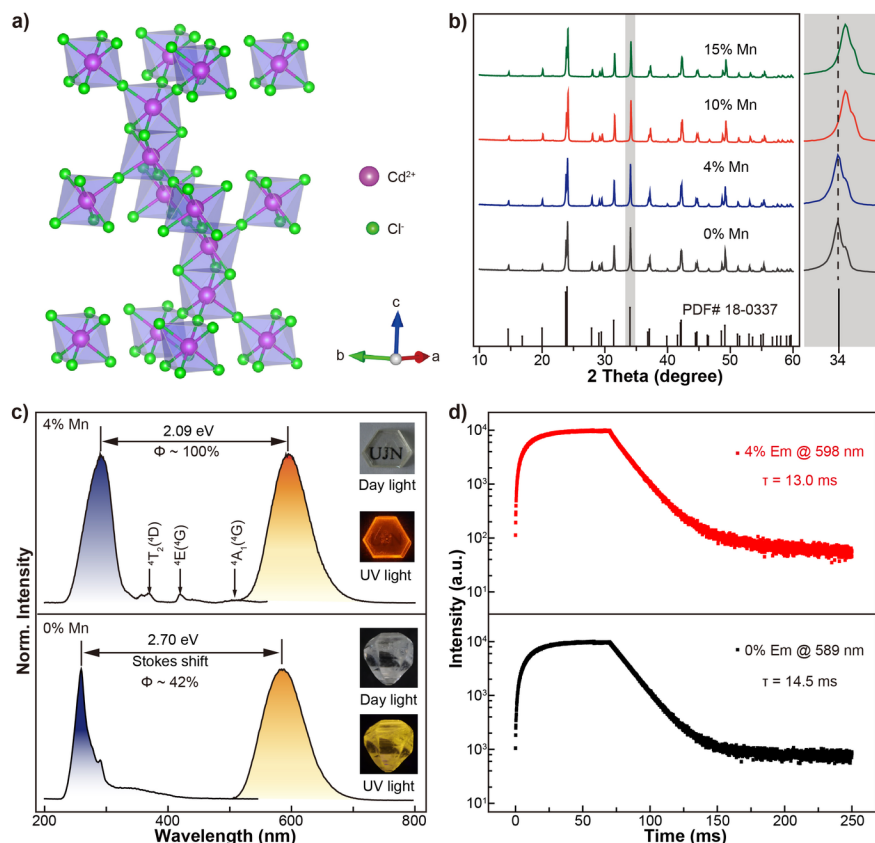


**FIGURE 1. Crystal structure and luminescence property of  $\text{CsCd}_{1-x}\text{Cl}_3:x\%$  Mn crystals.** (a) Schematic structure of  $\text{CsCdCl}_3$ . (b) XRD pattern suggested a pure phase after doping content up to 15%. (c) Steady-state photoluminescence excitation and emission spectrum before (bottom) and after (top) 4%  $\text{Mn}^{2+}$  doping. Insets are photographs of a crystal under day light and UV light, respectively. (d) Photoluminescence decay curves of  $\text{CsCdCl}_3$  and  $\text{CsCdCl}_3:4\%$  Mn crystals.

$\text{CsCdCl}_3$  single crystal was grown by a hydrothermal method.<sup>[17]</sup> Typically, powders of  $\text{CsCl}$  and  $\text{CdCl}_2$  (or a mixture with  $\text{MnCl}_2$ ) were stoichiometrically weighted and loaded in a vessel with Teflon lining. The vessel was then sealed in a steel cup and kept at 180 °C for 12 h in a muffle furnace, whereby the reagents were allowed to dissolve completely. The crystal growth was initiated by a slow cooling procedure from 180 °C to 30 °C at a rate of 3 °C/h. Transparent crystals at the bottom of vessel were then collected and rinsed with isopropanol before drying at room temperature (Figure S1). To identify the thermal stability of  $\text{CsCdCl}_3:4\%$  Mn, thermogravimetric analysis (TGA) test was performed in a temperature range from 30 to 1000 °C (Figure S2). There was no significant weight loss under 550 °C, suggesting a robust thermal stability.

$\text{CsCdCl}_3$  single crystal adapted a hexagonal structure (ICSD:16575) in a space group of  $\text{P6}_3/\text{mmc}$ ,<sup>[21]</sup> where a pair of face-sharing  $[\text{Cd}_2\text{Cl}_9]^{5-}$  octahedra were corn-connected with the other six  $[\text{CdCl}_6]^{4-}$  octahedra (Figure 1a), as further evidenced by the powder X-ray diffraction (XRD) measurement. Importantly, the crystal structure retained after heavy doping of  $\text{Mn}^{2+}$  up to 15 mol%, largely due to the similarity of ionic

valence between  $\text{Cd}^{2+}$  and  $\text{Mn}^{2+}$ . To probe the actual concentration of Mn ions in lattice, energy dispersive spectroscopy (EDS) measurement was performed (Figure S3). The actual concentration showed a linear increase with increasing nominal doping content, although a substantial deviation was also observed. Owing to their identical valence, the  $\text{Mn}^{2+}$  likely substituted the lattice site of  $\text{Cd}^{2+}$ . Since  $\text{Mn}^{2+}$  (0.67 Å) ion was significantly smaller than  $\text{Cd}^{2+}$  (0.96 Å), the substitution was further confirmed by the shrinkage of unit cell, as shown in XRD where the (204) peak shifted towards high angle (Figure 1b). Before doping, the pristine crystals were transparent in visible region as a result of the wide bandgap (4.80 eV) (Figure S4). After doping of  $\text{Mn}^{2+}$ , however, the crystal showed a pink tint which further deepened as dopant content increased (Figure S5).

Unlike their changed color, the photoluminescence of  $\text{CsCdCl}_3$  and  $\text{CsCdCl}_3:4\% \text{Mn}^{2+}$  single crystals were essentially identical under UV lamp excitation (Figure 1c). The pristine crystal showed an orange photoluminescence (PL) at 589 nm with a full-width-at-half-maximum (FWHM) of 78 nm and a sharp photoluminescence excitation (PLE) peak at 258 nm, leading to an extremely large Stokes shift up to 2.70 eV. After doping, the major excitation peak shifted from 258 nm to 292 nm. Besides, a series of weak excitation peaks emerged, which was ascribed to the  $d-d$  transition of  $\text{Mn}^{2+}$ .<sup>[18, 22]</sup> The emission peak slightly shifted to 598 nm with a Stokes shift up to 2.09 eV. Importantly, the PL QY was improved from 42% to  $\sim 100\%$  after 4-mol%  $\text{Mn}^{2+}$  doping. To understand such PL improvement, emission lifetime measurement was conducted (Figure 1d). Interestingly, the lifetime slightly decreased from 14.5 ms to 13.0 ms, suggesting no significant change. We further collected the excitation maps of both samples, and found a large overlap between two excitation centers (Figure S6). Such resonant emission centers could be ascribed to  $\text{Cd}^{2+}$  ( $^3\text{E}_g - ^1\text{A}_{1g}$ ) and  $\text{Mn}^{2+}$  ( $^4\text{T}_1 - ^6\text{A}_1$ ), respectively, featuring a common forbidden  $d-d$  transition.<sup>[22]</sup> Compared to self-trapped exciton,<sup>[23]</sup>  $\text{Cd}^{2+}$  ions were more likely responsible for the yellow emission of millisecond lifetime.<sup>[24]</sup> Therefore, the doping of  $\text{Mn}^{2+}$  passivated the non-radiative channel of  $\text{Cd}^{2+}$  by a fast resonant energy transfer, resulting in a boosted PL QY.

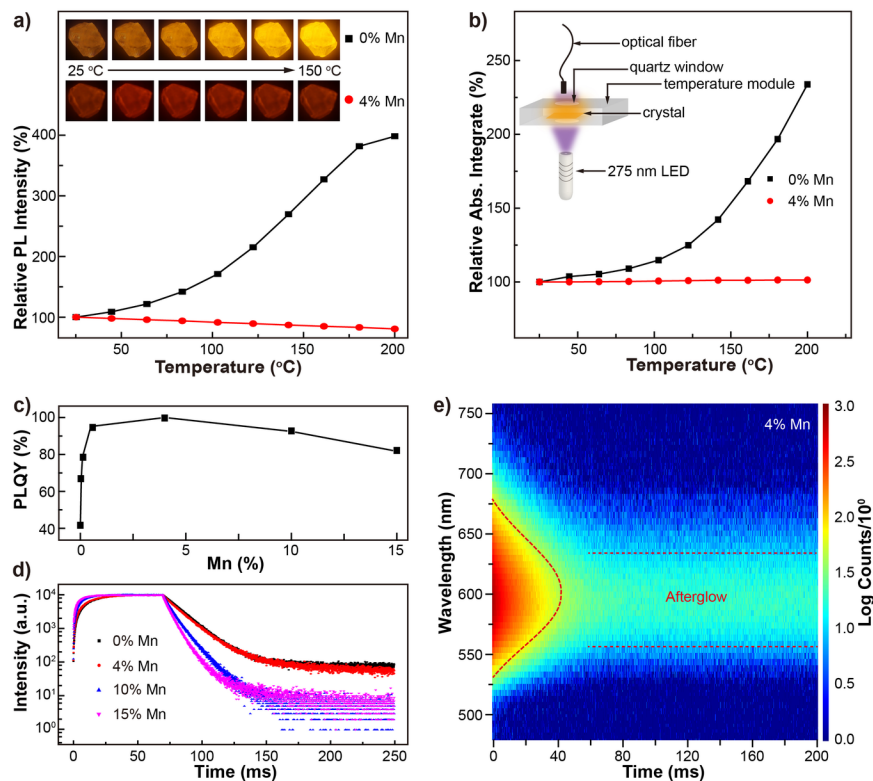


**FIGURE 2. Temperature-dependent and time-resolved photoluminescence of  $\text{CsCd}_{1-x}\text{Cl}_3:x\%$  Mn crystals.** Temperature-dependent PL (a) and absorption (b) spectra. Insets showed the luminescent photographs at varied temperatures. A 275-nm LED was used as the excitation source. (c) PL QY was plotted against  $\text{Mn}^{2+}$ -doping content, suggesting an optimal doping at 4 mol%. (d) The PL decay curves at varied doping contents indicated a concentration quenching at heavy doping level. (e) Time-resolved PL spectra within a time window of 200 ms, showing a clear trace of afterglow signal.

As mentioned above, the PL behavior between  $\text{Cd}^{2+}$  and  $\text{Mn}^{2+}$  were almost identical regarding to band width, peak position, and even lifetime. However, they showed a large difference in temperature-dependent luminescence. As shown in Figure 2a, the pristine crystal exhibited a substantial enhancement in PL intensity at high temperature while the doped crystal remained almost identical. To shed more light on their difference, the temperature-dependent PL spectra were collected in a temperature range from 25 to 200°C (Figure S7). Indeed, the PL intensity of pristine crystals increased strikingly by 4 folds while that of the doped one decreased by 20%, which was in good agreement with the photographs (Figure 2a, Figure S8). The PL decrease was readily ascribed to thermal quenching, yet the 4-fold enhancement remained to be explained.

To understand such an unusual enhancement, temperature-dependent absorption at 275 nm was conducted in a homemade temperature module (Figure 2b). The incident light intensity of a 275-nm LED before and after the doped crystal was recorded with varied temperature, and the difference was considered as the absorbed portion. Surprisingly, the absorption of the pristine crystals increased by 2.3 folds from 25 °C to 200 °C while that of the doped one remained almost constant. In this sense, the additional thermal-induced absorption was the major factor for the 4-fold enhancement of PL. Note that the such temperature dependence of absorption has been well documented in many semiconductors, such as crystalline silicon<sup>[25]</sup> and  $\text{CH}_3\text{NH}_3\text{PbI}_3$ .<sup>[26]</sup> Another possible factor could be the phonon-assisted processes, which stimulated the trapped excitons to radiative channel.<sup>[27, 28]</sup> The boosted PL QY eventually enhanced the PL intensity by the residual 1.7-fold. Based on this assumption, the PL QY of pristine crystals were 73% at 200°C.

Apart from phonon-assisted process,  $\text{Mn}^{2+}$ -doping content was found a facile tool to boost the PL QY of crystals. To this end, a series of  $\text{Mn}^{2+}$ -doped crystals were grown for an optimal doping concentration (Figure 2c). The PL QY increased from 42% to 100% when doping content increased from 0 to 4 mol%, followed by dropping to 80% at heavy doping of 15 mol%. To investigate the PL QY dropping, lifetime measurement at  $\sim 600$  nm was conducted for varied doping content (Figure 2d). The decay curves showed that with the  $\text{Mn}^{2+}$  content increasing from 0% to 15%, the lifetime decreased from 14.5 to 5.7 ms. It was attributed to the concentration quenching effect, whereby excitation energy was migrated to quenching sites via multiple cross-relaxation processes.<sup>[29, 30]</sup> Surprisingly, time-resolved PL mapping in the range from 480 nm to 760 nm demonstrated a clear afterglow feature of  $\text{CsCdCl}_3:4\%$   $\text{Mn}^{2+}$  crystals. Two kinds of decay centers were clearly distinguished in time domain, including a Gaussian profile at 598 nm of PL decay and an ultralong afterglow trace extending to 0.2 s (Figure 2e).

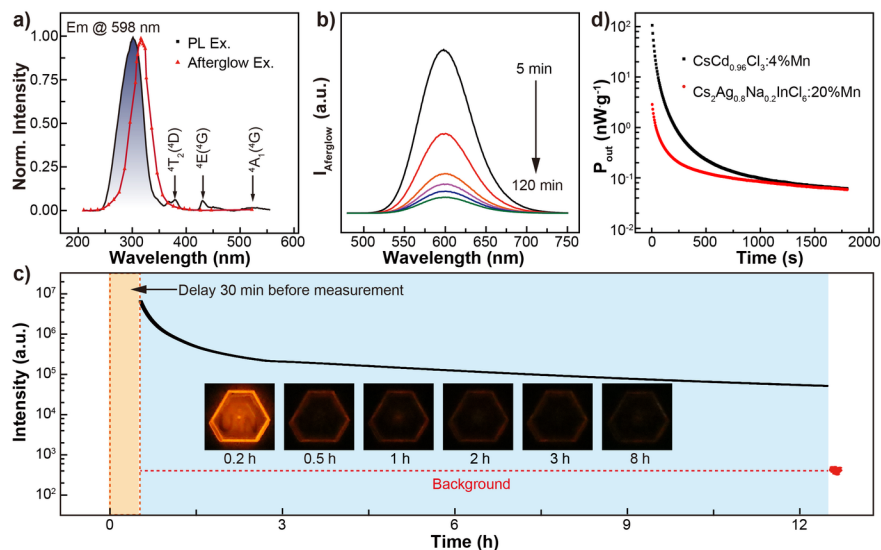


**FIGURE 3. Ultralong afterglow from CsCdCl<sub>3</sub>:4% Mn<sup>2+</sup> single crystal.** (a) Steady-state excitation spectra of PL and afterglow from crystal, showing a significant shift. (b) Afterglow spectra at different time delay after ceasing the excitation. (c) The afterglow decay curve showed an intense signal over background even after 12-hour delay. Note that a 30-min delay after ceasing excitation was used to avoid detector saturation. Insets were the afterglow photographs of a typical crystal. (d) A comparison of afterglow output power between two crystals.<sup>[17]</sup>

To shed more light on the afterglow of CsCdCl<sub>3</sub>:4% Mn<sup>2+</sup> crystals, excitation spectra for both PL and afterglow were measured. Note that, the afterglow excitation was obtained by plotting afterglow intensity against varied excitation light source<sup>[31]</sup> (Figure 3a, Figure S9, Table S1). Intriguingly, afterglow excitation spectrum showed a red shift of 0.26 eV when compared with PL excitation. In addition, direct excitation of Mn<sup>2+</sup> at 370, 420, and 515 nm failed to charge afterglow traps, indicating that the afterglow originated from the resonant energy transfer process from Cd<sup>2+</sup> to Mn<sup>2+</sup>. To identify the emitting center of afterglow, afterglow PL spectra were recorded at varied time interval after ceasing the excitation (Figure 3b). The afterglow spectra featured a Gaussian profile centering at 598 nm which hardly changed with decay time, indicating that the afterglow emitter was Mn<sup>2+</sup>(<sup>4</sup>T<sub>1</sub>-<sup>6</sup>A<sub>1</sub>) in nature. The afterglow intensity remained two orders of magnitude higher than the background noise after 12-hour decay (Figure 3c), which was amongst the most durable afterglow phosphors to the best of our knowledge.<sup>[32-34]</sup> In contrast, the afterglow duration of the pristine crystal was quite limited (a few minutes) (Figure S10). Remarkably, afterglow curve showed that the initial brightness of CsCdCl<sub>3</sub>:4% Mn<sup>2+</sup> was about 40 times higher than that of the first afterglow perovskite,<sup>[17]</sup> namely, Cs<sub>2</sub>Ag<sub>0.8</sub>Na<sub>0.2</sub>InCl<sub>6</sub>:20% Mn<sup>2+</sup> single crystals. (Figure 3d).

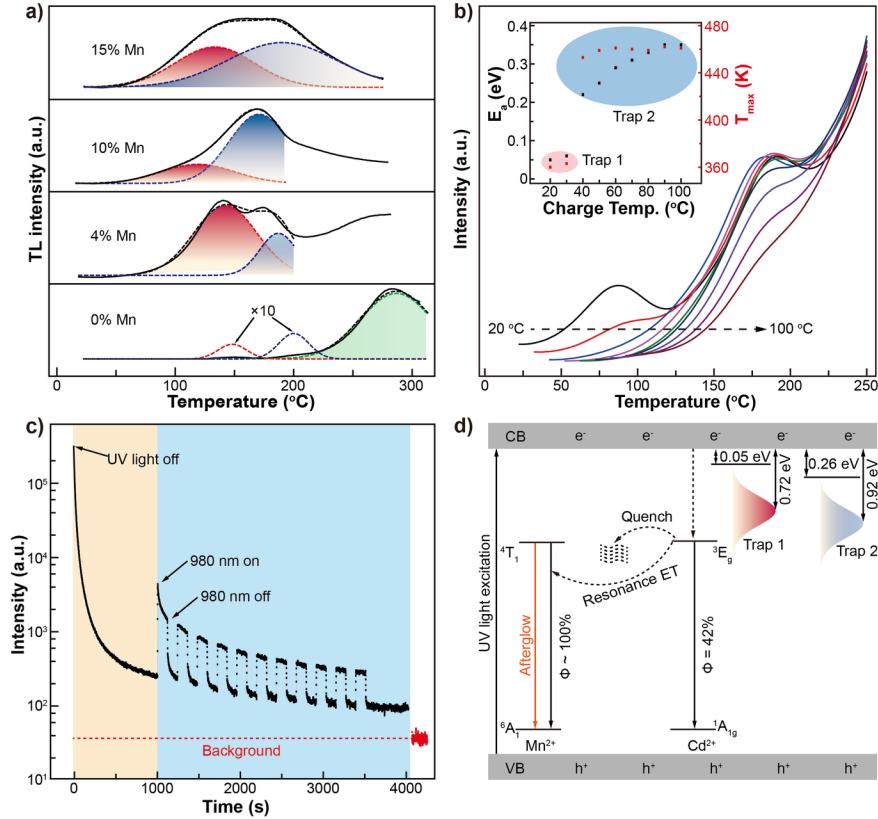


**FIGURE 4. Afterglow mechanism of CsCdCl<sub>3</sub>:4% Mn<sup>2+</sup> crystal.** (a) Thermoluminescence curves from 25°C to 300 °C. at a temperature ramping rate of 4 °C/s. (b) Thermoluminescence curves measured at different charging temperatures from 20 °C to 100 °C. Inset was the calculated trap distribution by two distinct methods, including thermal cleaning method and initial rise method. (c) Afterglow decay trace after ceasing excitation, where the spikes were the stimulated signal with a 980-nm laser. (d) Afterglow mechanism involving two traps was proposed.

To understand the ultralong afterglow mechanism of crystals, the thermoluminescence (TL) curves of CsCd<sub>1-x</sub>Cl<sub>3</sub>:x% Mn<sup>2+</sup> crystals were measured (Figure 4a). The pristine CsCdCl<sub>3</sub> crystal exhibited an ultra-deep trap at 280 °C. Interestingly, the trap disappeared after 4-mol% Mn<sup>2+</sup> doping. Meanwhile two shallow traps at 140 °C and 180°C emerged significantly, which shifted slightly towards low-temperature end after heavy doping at 10 mol% and 15 mol%. To investigate the distribution of traps, TL curves of a typical crystal were measured at different charging temperature (Figure 4b, Figure S11). The initial rise method was then used to estimate the top edge of two kinds of traps, suggesting a shallowest level at 0.05 eV and 0.26 eV, respectively. Based on the thermal-cleaning method, the average depths of traps were calculated to be 0.72 eV to 0.92 eV, respectively.<sup>[35]</sup> As shown in Figure 4b inset, the two traps were discretely distributed with an energy difference about 0.2 eV (Supporting Video), which echoed well with difference between PL and afterglow excitation (Figure 3a). In this sense, we speculated that the afterglow could be charged more effectively by direct filling of deep traps which has a shallow edge exactly below conduction band by 0.26 eV. In addition to thermal excitation, trapped electrons in crystal could also be stimulated and released by photoexcitation at 980 nm which has a sufficient energy (~ 1 eV) to the trap depth (Figure 4c). After multiple cycles of photon stimulation (4-min for each cycle), the afterglow intensity was still about an order of magnitude higher than the background noise. Both the multiple-cycle photon stimulation and the long-term thermoluminescence (Supporting Video) suggested a large density of traps.

Based on the above discussion, both the luminescence and afterglow mechanism were proposed as shown in Figure 4d. Before  $\text{Mn}^{2+}$  doping, electrons in the conduction band mainly have two transition routes: one part of electrons radiatively transitioned to  $^3\text{E}_g$  energy level of  $\text{Cd}^{2+}$  while the other part were non-radiatively quenched by defects, leading to a low PL QY about 42%. After  $\text{Mn}^{2+}$  doping, the latter route involving quenching was outperformed by the rapid resonant energy transfer from  $\text{Cd}^{2+}$  to  $\text{Mn}^{2+}$  due to their almost identical bandgap. In this sense, the PL QY was significantly boosted as a result of the high efficiency of radiative  $d-d$  transition from  $\text{Mn}^{2+}$ . As to the afterglow, two kinds of traps below bandgap were illustrated in Figure 4d. Upon thermal perturbation, the trapped electrons were elevated to conduction band, followed by relaxation to nearby  $\text{Cd}^{2+}$  due to its rich content (97.5-mol%). Thereafter, the  $\text{Mn}^{2+}$  acceptor was excited by resonant energy transfer from  $\text{Cd}^{2+}$  donor, whereby a strong afterglow was generated.

In conclusion, a new optical host for afterglow, namely  $\text{CsCdCl}_3$ , was grown in a hydrothermal reactor. The pristine crystal showed a relatively PL QY at room temperature, which was further boosted up to 73% at 200 °C. After  $\text{Mn}^{2+}$  doping, the PL QY was further elevated to 100% due to the efficient resonant energy transfer from  $\text{Cd}^{2+}$  to  $\text{Mn}^{2+}$ . Importantly, an ultralong afterglow up to 12 hours were observed for the doped crystals, which was attributed to the interplay between two kinds of traps based on TL measurement. This work brought a new member to the library of transparent afterglow crystal, opening many possibilities to advanced applications such as volumetric display and three-dimensional information encryption.

### Acknowledgments

This work is financially supported by the Natural Science Foundation of Shandong Province (No. ZR2020YQ12), Young Taishan Scholars Program of Shandong Province (No. tsqn201812082).

### References

1. K. Huang, X. Dou, Y. Zhang, X. Gao, J. Lin, J. Qu, Y. Li, P. Huang, G. Han, *Adv. Funct. Mater.* **2021**, *31*, 2009920.
2. Y. M. Yang, Z. Y. Li, J. Y. Zhang, Y. Lu, S. Q. Guo, Q. Zhao, X. Wang, Z. J. Yong, H. Li, J. P. Ma, Y. Kuroiwa, C. Moriyoshi, L. L. Hu, L. Y. Zhang, L. R. Zheng, H. T. Sun, *Light Sci. Appl.* **2018**, *7*, 88.
3. Z. Pan, Y. Y. Lu, F. Liu, *Nat. Mater.* **2011**, *11*, 58.
4. X. Wang, Y. Chen, F. Liu, Z. Pan, *Nat. Commun.* **2020**, *11*, 2040.
5. N. Liu, W. Zheng, R. Sun, X. Li, X. Xie, L. Wang, Y. Zhang, *Adv. Funct. Mater.* **2021**, *32*, 2110663.
6. J. Han, W. Feng, D. Y. Muleta, C. N. Bridgmohan, Y. Dang, G. Xie, H. Zhang, X. Zhou, W. Li, L. Wang, D. Liu, Y. Dang, T. Wang, W. Hu, *Adv. Funct. Mater.* **2019**, *29*, 1902503.
7. J. Ueda, S. Miyano, S. Tanabe, *ACS Appl. Mater. Interfaces* **2018**, *10*, 20652.
8. S. Das, S. K. Sharma, J. Manam, *Ceram. Int.* **2022**, *48*, 824.
9. X. Ou, X. Qin, B. Huang, J. Zan, Q. Wu, Z. Hong, L. Xie, H. Bian, Z. Yi, X. Chen, Y. Wu, X. Song, J. Li, Q. Chen, H. Yang, X. Liu, *Nature* **2021**, *590*, 410.
10. V. Liepina, D. Millers, K. Smits, *J. Lumin.* **2017**, *185*, 151.
11. Y. Gao, R. Li, W. Zheng, X. Shang, J. Wei, M. Zhang, J. Xu, W. You, Z. Chen, X. Chen, *Chem. Sci.* **2019**, *10*, 5452.
12. Y. Zhuang, Y. Lv, Y. Li, T. Zhou, J. Xu, J. Ueda, S. Tanabe, R. J. Xie, *Inorg. Chem.* **2016**, *55*, 11890.
13. Q. Cheng, Y. Wang, L. Su, H. Wang, G. Zhu, W. Yu, *J. Mater. Chem. C* **2019**, *7*, 4567.
14. Y. Liang, F. Liu, Y. Chen, K. Sun, Z. Pan, *Dalton Trans.* **2016**, *45*, 1322.
15. C. Mével, J. Carreaud, G. Delaizir, J.-R. Duclère, F. Brisset, J. Bourret, P. Carles, C. Genevois, M. Allix,

- S. Chenu, *J. Eur. Ceram. Soc.* **2021**, *41*, 4934.
16. H. Tang, S. Liu, Z. Fang, Z. Yang, Z. Cui, H. Lv, P. Zhang, D. Wang, F. Zhao, J. Qiu, X. Yu, X. Xu, *Adv. Opt. Mater.* **2022**, *10*, 2102836.
17. W. Zheng, X. Li, N. Liu, S. Yan, X. Wang, X. Zhang, Y. Liu, Y. Liang, Y. Zhang, H. Liu, *Angew. Chem. Int. Ed.* **2021**, *60*, 24450.
18. X. Chen, X. Wang, X. Zhang, Y. Zhang, *J. Phys. Chem. Lett.* **2022**, *13*, 8163.
19. Y. Shi, X. Zhang, X. Chen, Y. Zhang, *ChemComm.* **2022**, *58*, 10048.
20. X. Wang, X. Zhang, S. Yan, H. Liu, Y. Zhang, *Angew. Chem. Int. Ed. Engl.* **2022**, *61*, e202210853.
21. R. Demirbilek, R. Feile, A. Çelik Bozdoğan, *J. Lumin.* **2015**, *161*, 174.
22. B. Yang, X. Mao, F. Hong, W. Meng, Y. Tang, X. Xia, S. Yang, W. Deng, K. Han, *J. Am. Chem. Soc.* **2018**, *140*, 17001.
23. S. He, Q. Qiang, T. Lang, M. Cai, T. Han, H. You, L. Peng, S. Cao, B. Liu, X. Jing, B. Jia, *Angew. Chem. Int. Ed. Engl.* **2022**, e202208937.
24. Z. Tang, R. Liu, J. Chen, D. Zheng, P. Zhou, S. Liu, T. Bai, K. Zheng, K. Han, B. Yang, *Angew. Chem. Int. Ed. Engl.* **2022**.
25. A. Poruba, J. Springer, L. Mullerova, A. Beitlerova, M. Vaněček, N. Wyrsh, A. Shah, *J Non Cryst Solids.* **2004**, *15*, 222.
26. C. Barugkin, J. Cong, T. Duong, S. Rahman, H. T. Nguyen, D. Macdonald, T. P. White, K. R. Catchpole, *J. Phys. Chem. Lett.* **2015**, *6*, 767.
27. J. Qiao, L. Ning, M. S. Molokeev, Y. C. Chuang, Q. Liu, Z. Xia, *J. Am. Chem. Soc.* **2018**, *140*, 9730.
28. B. B. Zhang, J. K. Chen, J. P. Ma, X. F. Jia, Q. Zhao, S. Q. Guo, Y. M. Chen, Q. Liu, Y. Kuroiwa, C. Moriyoshi, J. Zhang, H. T. Sun, *J. Phys. Chem. Lett.* **2020**, *11*, 2902.
29. E. Song, S. Ye, T. Liu, P. Du, R. Si, X. Jing, S. Ding, M. Peng, Q. Zhang, L. Wondraczek, *Adv. Sci. (Weinh).* **2015**, *2*, 1500089.
30. J. Wang, F. Wang, C. Wang, Z. Liu, X. Liu, *Angew. Chem. Int. Ed. Engl.* **2011**, *50*, 10369.
31. J. Du, K. Li, R. Van Deun, D. Poelman, H. Lin, *Adv. Opt. Mater.* **2021**, *10*, 2101714.
32. F. Liu, Y. Chen, Y. Liang, Z. Pan, *Opt. Lett.* **2016**, *41*, 954.
33. M. Ma, L. Li, C. Cai, Y. Han, Y. Yang, *J. Lumin.* **2022**, *252*, 119376.
34. J. Wang, B. Liu, W. Chen, Q. Qiang, L. Peng, T. Han, T. Zeng, Z. Zhou, Z. Yang, Y. A. Nikolaevich, *J. Lumin.* **2022**, *243*, 118644.
35. A. Feng, J. J. Joos, J. Du, P. F. Smet, *Phys. Rev. B* **2022**, *105*, 205101.